UC San Diego
UC San Diego Previously Published Works

Title

Dispersion curve estimation via phased array beamforming methods

Permalink

https://escholarship.org/uc/item/3n33s383

Journal

Journal of Intelligent Material Systems and Structures, 25(5)

ISSN

1045-389X

Authors

Jarmer, Gregory J
Flynn, Eric B
Todd, Michael D

Publication Date

2014-03-01

DOI

10.1177/1045389x13494930

Peer reviewed

Dispersion curve estimation via phased array beamforming methods

Gregory J Jarmer, Eric B Flynn and Michael D Todd

Published by:

$SAGE

http://www.sagepublications.com

Additional services and information for *Journal of Intelligent Material Systems and Structures* can be found at:

Email Alerts: http://jim.sagepub.com/cgi/alerts

Subscriptions: http://jim.sagepub.com/subscriptions

Reprints: http://www.sagepub.com/journalsReprints.nav

Permissions: http://www.sagepub.com/journalsPermissions.nav

>> OnlineFirst Version of Record - Jul 11, 2013

What is This?

Dispersion curve estimation via phased array beamforming methods

Gregory J Jarmer[1], Eric B Flynn[2] and Michael D Todd[1]

Abstract
Localization of scattering sources via active ultrasonic inspection in plate-like structures requires knowledge of the structure's dispersion relation and material properties. Often the dispersion relation and material properties are unknown, uncertain, or difficult to model due to material complexity and variability in material properties, geometry, and/or environment, thereby requiring in situ estimation. Two methods are presented for estimating guided wave dispersion curves (phase and group velocity) in a multimodal, multipath environment using a phased array. Phase and group velocities are estimated in situ on an aluminum and carbon fiber plate and compared to theoretical values. Scattering from plate boundaries is localized using the estimated phase and group velocity curves through beamforming and ranging via time of flight.

Introduction

Detection, localization, and characterization of scattering sources using guided ultrasonic waves are of long-standing interest in the fields of structural health monitoring (SHM) and nondestructive evaluation (NDE). This is due to the ability of guided waves to inspect large structural areas and their sensitivity to defects (Alleyne and Cawley, 1992; Rose, 2002). Inspection techniques are often implemented via an active sensing scheme, where the scattered spatiotemporal wave field is sampled by an array of transducers and analyzed using various signal processing techniques (Clarke et al., 2009; Giurgiutiu and Bao, 2004). Accurate knowledge of the structure's dispersion (frequency–velocity) curves is vital to any signal processing algorithm: phase velocity for direction of arrival estimation in beamforming algorithms and group velocity for ranging the scattering location. Under idealized conditions, (material properties, geometry, and operating environment known), theoretical dispersion curves may be solved for using advanced numerical methods (Lowe, 1995). However, in practice, a structure is never ideal, and there is always uncertainty associated with known parameters. The practical implementation of SHM/NDE inspection techniques for these cases requires in situ estimation of dispersion curves. This research focuses on the use of phased arrays to estimate phase velocity (frequency–wavenumber) and group velocity curves in situ for multipath, multimodal plate structures.

Numerous methods have been investigated for estimation of phase velocity curves. Frequency–wavenumber curves for plate waves were determined experimentally (Hutchins et al., 1989; Schumacher et al., 1993) and theoretically (Hall and Michaels, 2010) using a phase spectral analysis technique first developed by Sachse and Pao (1978) for determining phase and group velocities in solids. Here, relation between the phases of a signal at two sensor locations is used to calculate phase velocity. Difficulty arises in implementing these techniques if the number of plate modes is unknown or the modes are not separated sufficiently in time, which is often the case in multipath environments such as plate structures.

Multidimensional discrete Fourier transform (DFT) techniques were used by several researchers to determine frequency–wavenumber curves of plate modes, whereby array data (sampled in both time and space) are decomposed into frequency–wavenumber components (Alleyne and Cawley, 1991; Kley et al., 1999). A

[1]Department of Structural Engineering, University of California, San Diego, La Jolla, CA, USA
[2]Los Alamos National Laboratory, Los Alamos, NM, USA

Corresponding author:
Michael D Todd, Department of Structural Engineering, University of California, San Diego, 8500 Gilman Drive 0085, La Jolla, CA 92093-0085, USA.
Email: mdtodd@ucsd.edu

major advantage of the multidimensional DFT is that plate modes can overlap in time allowing for its use in multipath environments. However, major disadvantages are the spatial Nyquist sampling criteria set by the inter-element array spacing and the requirement of linearly spaced elements for implementation of the spatial DFT, which limits use to rectilinear linear array geometries.

Group velocity curves are often determined experimentally for a narrowband pulse using estimated time of flight in conjunction with known distance traveled. Time of flight is estimated by peak picking the envelope of a received waveform (Michaels and Michaels, 2007). As with phase velocity estimation, difficulty occurs in multipath, multimodal environments when wave packets overlap in time and the number modes are unknown.

Group velocity is also estimated using time–frequency representations (Niethammer et al., 2001; Prosser et al., 1999). Here, a signal's frequency content is analyzed as a function of time allowing for identification of individual wave modes that overlap in time. Group velocity is again estimated by time of flight peak picking in conjunction with known distance traveled. One of the few disadvantages of the time–frequency representations is the difficulty of identifying time of flight peaks for a multipath environment where reflections cause interference.

This article presents two phased array beamforming techniques to allow in situ estimation of phase and group velocity curves in a multimodal, multipath environment. Phase velocity is estimated via a narrowband wavenumber beamforming technique, applicable to any array geometry provided that temporal and spatial Nyquist sampling criteria are satisfied. The contribution of this technique is that it carries the advantages associated with the multidimensional DFT techniques without the requirement of rectilinear array element spacing. Group velocity curves are estimated through phased array beamforming; a desired mode is amplified while interfering/undesired modes are attenuated. The contribution of the technique is that it allows for enhanced identification of modal peaks when multiple modes and reflections are present.

The organization of this article is as follows: The problem statement and assumptions made concerning the wave propagation environment are first discussed followed by a brief overview of frequency–wavenumber decomposition for a multimodal signal via the multidimensional Fourier transform. Techniques for estimating phase and group velocity via phased array beamforming are presented and discussed. Experimental results are presented with application for both an aluminum plate and a carbon fiber plate. Estimated dispersion curves for the aluminum plate are compared to theoretical values and used to image boundary reflections. The effect of reduced array size

on estimating phase and group velocity is also explored. Estimated dispersion curves for the carbon fiber plate are used to image boundary reflections, taking into account material anisotropy. The highlights of this article and limitations of the proposed methods are discussed.

Problem statement

The problem examined and experimental setup is illustrated in Figure 1 for a multimodal multipath environment. An active sensing scheme is used to detect the location of damage in a plate structure where a single actuation transducer interrogates the plate with a narrowband pulse while an array of N sensors measures the scattered wave field at positions $\vec{x}_i$ ($i = 0, 1 \ldots N - 1$). The output of each sensor is represented as $f_i(t)$. The phase and group velocities for the plate are unknown due to uncertainty in material properties, geometry, and environmental conditions and must be estimated in situ. Due to the location of the array and the multipath environment, plate modes excited by the actuator overlap in time and cannot be easily gated in time.

It is assumed that scattering occurs in the far field, and the resulting wave is represented as a plane wave of the form

$$s(\vec{x}, t) = \exp\left(j \left(\omega_0 t - \vec{k}_0 \vec{x} \right) \right) \tag{1}$$

where ω_0 is temporal frequency coinciding with the center frequency of the actuation pulse and $\vec{k}_0$ is the wave vector. The wave vector has components of $\vec{k}_0 = (2\pi/\lambda)[\cos(\theta), \sin(\theta)]$, where λ is wavelength and

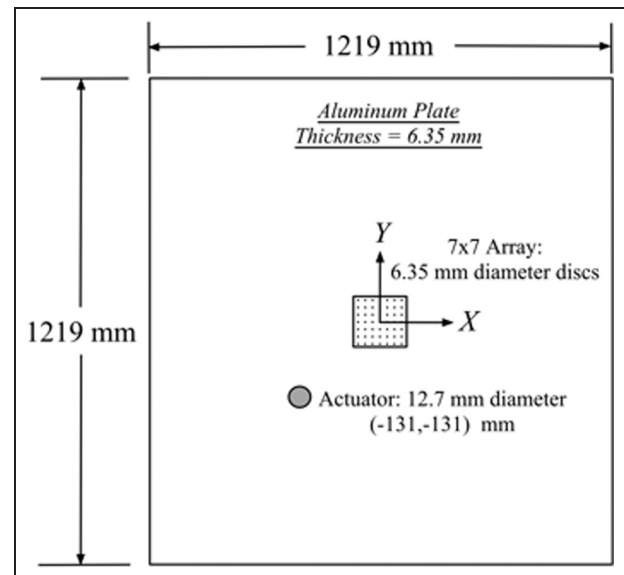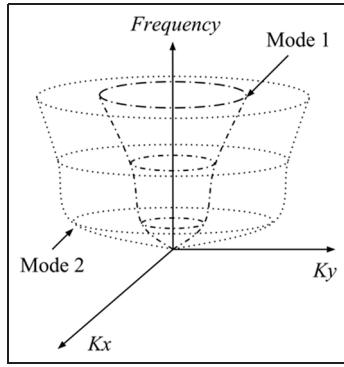**Figure 1.** Problem examined and experimental setup for aluminum plate experiment.

Figure 2. Frequency–wavenumber space for multimodal signal.

θ is measured clockwise from the X-axis. The magnitude of the wave vector is known as wavenumber, $\left|\vec{k}_0\right| = k_0$, and represents the spatial frequency in the direction of propagation. Assuming ideal sampling, $f_i(t) = s(\vec{x}_i, t)$. It is noted that the phase of scattered plan wave is measured relative to the origin of the coordinate system and will differ from sensor to sensor. The signal processing techniques discussed in the following sections use the relative phase difference between sensors and don't require knowledge of the actual phase.

Frequency–wavenumber components

Here, to aid in the explanation of the proposed phased array beamforming techniques, the frequency–wavenumber components of a multimodal field are examined.

Multimodal isotropic wave field

The complex plane wave from (1) is decomposed into frequency–wavenumber components through the multidimensional Fourier transform

$$
\begin{aligned}
S\left(\omega, \vec{k}\right) &= \int_{-\infty}^{\infty}\int_{-\infty}^{\infty}\int_{-\infty}^{\infty}\int_{-\infty}^{\infty} s(\vec{x}, t)\exp\left(-j\left(\omega t - \vec{k}\vec{x}\right)\right)d\vec{x}dt \\
&= \int_{-\infty}^{\infty}\int_{-\infty}^{\infty}\int_{-\infty}^{\infty}\int_{-\infty}^{\infty}\exp\left(j\left(\omega_0 t - \vec{k}_0\vec{x}\right)\right) \\
&\quad \exp\left(-j\left(\omega t - \vec{k}\vec{x}\right)\right)d\vec{x}dt \\
&= \delta\left(\vec{k} - \vec{k}_0\right)\delta\left(\omega - \omega_0\right)
\end{aligned}
\tag{2}
$$

A plane wave transforms to a single point in frequency–wavenumber space at location ($\omega = \omega_0$, $\vec{k} = \vec{k}_0$). Each point in frequency–wavenumber space corresponds to a plane wave in space–time, with a particular orientation and frequency. Figure 2 is a representation of two theoretical plate modes in frequency–wavenumber space, where the shape of each modal surface is governed by the dispersion relation for the
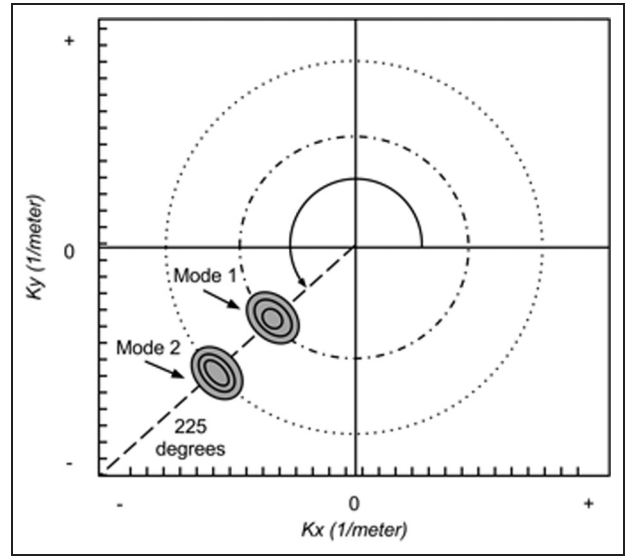

Figure 3. Frequency slice from frequency–wavenumber surface showing two modes arriving at an angle of 225°.

material. At planes of constant frequency, each mode traces out a circle due to constant phase velocity and arbitrary propagation direction. The radius for each mode is determined by its dispersion relation for the given frequency ($k_1 = \omega_0 c_{p_1}$, $k_2 = \omega_0 c_{p_2}$), where c_p is the phase velocity of the respective mode. Frequency–wavenumber curves for a constant propagation direction are the intersection of a vertical plane with the modal surfaces. Figure 3 is a frequency slice of the frequency–wavenumber surface illustrating experimental data, where two modes are propagating from a direction of 225°.

Phase and group velocity are defined using the relations between frequency and wavenumber

$$
c_p = \frac{\omega}{k}, c_g = \frac{d\omega}{dk}
\tag{3}
$$

The phase velocity for an anisotropic material is a function of propagation angle, thus the phase velocity curves shown in Figure 3 are no longer necessarily circular. Additionally, the direction that the energy of waveform travels (group velocity) can differ from the direction of the phase velocity (Wang and Yuan, 2007).

Dispersion curve estimation

Phase velocity estimation via wavenumber beamforming

When sampling of the spatiotemporal field is not linearly spaced, spectral decomposition via the multidimensional DFT cannot be implemented. In this situation, the spectral components may be estimated by beamforming over wavenumber instead of angle when the direction of arrival is known. To see how this is

accomplished, it is first informative to illustrate how beamforming is able to estimate the arrival angle of an incoming narrowband wave. A beamformer applies time shifts to the received signals and sums

$$B(t) = \sum_{i=1}^{N-1} w_i f_i(t - \tau_i) \qquad (4)$$

Here, w_i is an array weighting function, and τ_i is the delay from an assumed arrival direction given as

$$\tau_i = -\frac{\vec{a}'\vec{x}_i}{c_p} \qquad (5)$$

where $\vec{a}$ is the assumed arrival direction of the signal and c_p is the known-phase velocity. If the actual signal propagating through the array is that of (1), the beamformer output is

$$\begin{aligned} B &= \sum_{i=1}^{N-1} w_i f_i(t - \tau_i) \\ &= \sum_{i=1}^{N-1} w_i s(\vec{x}_i, t + \vec{a}'\vec{x}_i/c_p) \\ &= \sum_{i=1}^{N-1} w_i \exp\left(j\left(\omega_0 \vec{a}'\vec{x}_i/c_p - \vec{k}'_0 \vec{x}_i\right)\right) \exp(j\omega_o t) \\ &= \sum_{i=1}^{N-1} w_i \exp\left(j\left(\vec{k}'_\beta \vec{x}_i - \vec{k}'_0 \vec{x}_i\right)\right) \exp(j\omega_o t) \end{aligned} \qquad (6)$$

where $\vec{k}_\beta = \omega_0 \vec{a}/c_p$. A beamformer estimates the arrival direction of a wave by "forming beams" over all possible arrival directions by shifting the received signals in time and summing. Beams that result in peaks are taken as estimates of arrival direction. For the example case in equation (6), beamforming at the arrival direction of $\vec{k}_0$ results in $\vec{k}_\beta = \vec{k}_0$ and $B(t) = N \exp(j\omega_0 t)$, where the weighting function w_i is equal to 1. The largest value of $B(t)$ is obtained by coherently combining the signals at each sensor with the resulting modulus equal to N. Any additional signals present in $f_i(t)$ such as reflections from boundaries or wave modes of different wavenumber will be incoherently combined. Thus, beamforming allows for separation of waves propagating through the array at the same time by exploiting a difference in arrival direction or wavenumber.

Beamforming in wavenumber estimates the spectral components of a waveform with known arrival direction by fixing $\vec{a}$ and beamforming over c_p. The peaks of the beamformed output are taken as estimates of the phase velocity of the modes present.

For an anisotropic material, the phase velocity is iteratively estimated to account for any difference between the assumed direction of wave propagation (direction of actuator) and actual direction due to anisotropy: (a) an initial phase velocity estimate for a mode is made assuming the propagation direction

coincides with actuator angle and by beamforming in wavenumber. This helps to reduce the propagation direction/phase velocity search space for mildly anisotropic materials by assuming that the phase velocity direction is close to that of the group velocity. (b) The estimated phase velocity is then used to estimate arrival direction of a mode by beamforming in angle over a range of permissible values. (c) The new arrival direction (replacing actuator direction) is then used to again estimate phase velocity. Mathematically, the iteration scheme is a repetition of equation (6), where the wavenumber space of a narrowband waveform is searched by scanning over arrival direction and phase velocity.

The processes of beamforming in angle and beamforming in wavenumber become clearer when viewing the operations on a frequency slice (Figure 3). Beamforming over angle is the process of tracing out the circular path with radius (wavenumber) corresponding to a known-phase velocity of the mode according to equation (3). Tracing either circle in Figure 3 results in a single peak corresponding to the mode's direction of arrival. Beamforming over wavenumber corresponds to tracing out a line with known arrival direction. If starting from the origin and tracing out a line at 225°, two peaks are encountered which serve as wavenumber estimates of the two modes. An important point to note is the assumption that the signal is narrowband in frequency, which allows for a time shift to be approximated by a phase shift. In practice, a phase shift is implemented either in the time domain on the analytic representation of the data or in the frequency domain on the narrowband frequency range of the data.

Figure 4 illustrates the experimental procedure to estimate frequency–wavenumber curves using a narrowband input with known arrival direction. First, the array data are decomposed into frequency components, and the narrowband frequency range corresponding to the actuation frequency is wavenumber-beamformed and averaged in magnitude. The resulting vector is an estimate of the wavenumber components for the center actuation frequency. The process is repeated for additional narrowband excitation frequencies to form a frequency–wavenumber surface. Once the surface is formed, the dominant peaks are extracted corresponding to the modes present. Phase velocity for a mode is calculated using equation (3).

Group velocity estimation via mode beamforming

Group velocity estimation for each mode found in the phase velocity estimate is accomplished by beamforming for the respective mode using the known arrival direction and estimated phase velocity on the narrowband analytic representation of the array data. For the multimode example illustrated in Figure 3, both the arrival direction (225°) and phase velocity (radius of
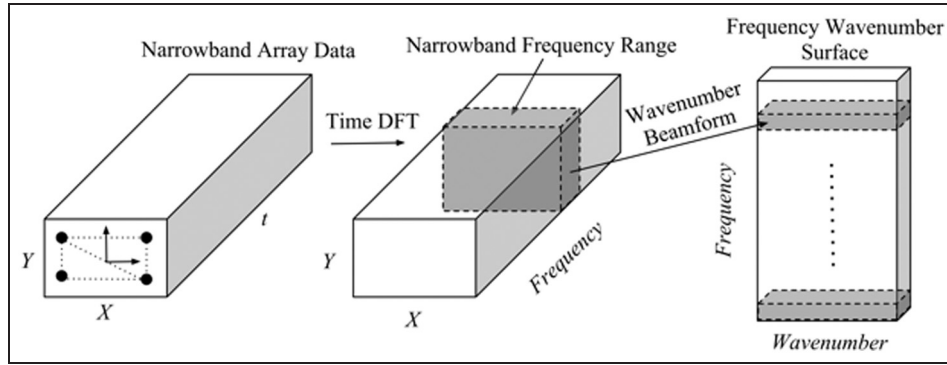
Figure 4. Experimental wavenumber beamforming procedure.
DFT: discrete Fourier transform.

circle) are known. As previously discussed and shown in equation (6), beamforming for a particular mode coherently combines sensor outputs, while multipath reflections and modes with a different phase velocity incoherently combine. This allows for time of flight identification by beamforming at each time sample and picking the maximum peak of the resulting beam-formed time series. Group velocity is then determined using the known distance traveled for each narrowband input measured relative to the origin of the array. It is important to note that the phase shift or time delay applied to each sensor is a relative shift measured from the array origin and that the peak of the beamformed time series occurs when the mode is present at all of the sensors. Estimating the group velocity via this process for an anisotropic material excited by broadband pulse and the array located in the near field of the actuator could potentially result in an inaccurate estimate due to additional phase delay caused by difference in the propagation direction between the phase and group velocities. This study assumes a far field wave field and a narrowband excitation limiting the proposed processing methods to these assumptions. An alternative method of estimating group velocity with phase velocity known is through the slope of the frequency–wavenumber curves. The slope can be estimated either numerically by direct evaluation of equation (3) or though curve fitting a function, such as a low-order rational polynomial, to the frequency–wavenumber curves and then taking the derivative. In practice, both of these approaches are very difficult to implement. Small errors in wavenumber estimates result in large changes in group velocity values when numerically evaluating the slope, and determining a generalized function that fits the shape and curvature of the non-linear frequency–wavenumber curves is difficult.

Experimental results

The frequency–wavenumber curves, phase velocity, and group velocity are estimated for an aluminum and carbon fiber plate to demonstrate the proposed estimation methods. The geometry and experimental setup for each are given in Figures 1 and 5. The array geometry for each experiment is the same with the largest inter-element spacing equal to 6.35 mm. This fixes the largest wavenumber before spatial aliasing to 78 m^{-1} or a shortest wavelength of 12.8 mm

$$\frac{2\pi}{d} = \frac{2\pi}{0.00635 \, \text{m}} \geq 2\Omega_{Spatial\ Nyquist} \Rightarrow$$
$$\Omega_{Spatial\ Nyquist} = 494 \, \text{rad} \cdot \text{m}^{-1} = 78 \text{m}^{-1} \qquad (7)$$

When performing the experiments, an initial frequency scan, range from 20 to 200 kHz at increments of 1 kHz, is used based upon theoretical frequency–wavenumber curves for the aluminum plate as a valid region where spatial aliasing would not occur. A 3.5-cycle Hamming windowed sine wave is used as the
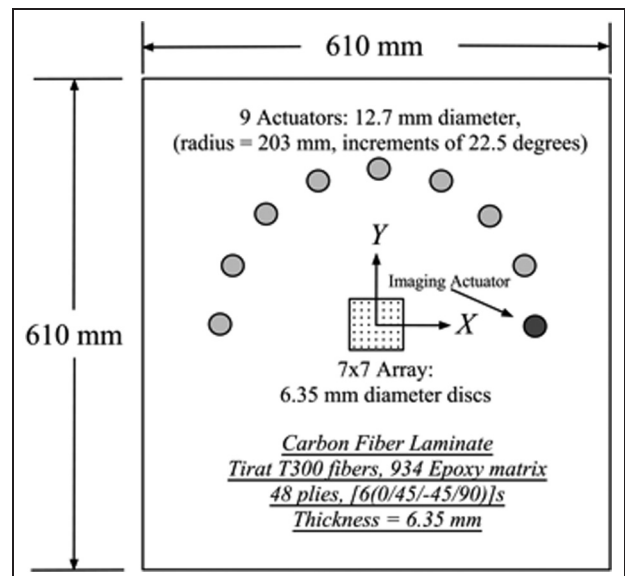

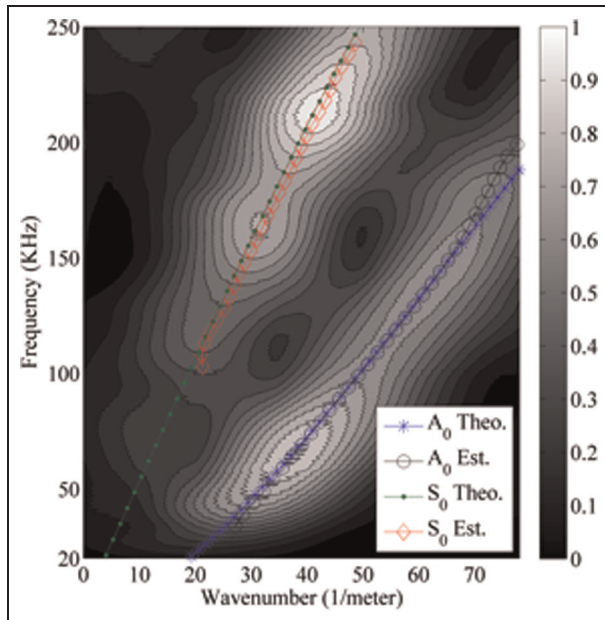**Figure 5.** Experimental setup for carbon fiber laminate plate experiment.

Figure 6. Frequency–wavenumber surface for aluminum plate with theoretical (Theo.) and estimated (Est.) curves.

Figure 7. Experimental and theoretical phase velocity for aluminum plate.

actuation signal and a 4 MHz sampling rate for acquisition. A rectangular array weighting function was used for all processing. Extracted curves for the aluminum plate are compared to theoretical predictions. Reflections from boundaries for both plates are imaged using the estimated phase and group velocity as means of experimentally checking accuracy.

Aluminum plate

An aluminum plate, as shown in Figure 1, is chosen as a test structure since it is representative of many aerospace components. It is noted that only a single actuator, located 225° relative of the array coordinate system, is used since the aluminum plate is homogeneous making the phase and group velocities independent of propagation direction. Additionally, the well-known Rayleigh–Lamb dispersion relations that govern the wave propagation provide a means for comparing extracted curves to theoretical values.

Phase velocity estimation. The frequency–wavenumber curves are extracted following the procedure illustrated in Figure 4. The frequency–wavenumber surface, where color amplitude represents normalized power (magnitude squared value of resulting complex signal), is shown in Figure 6 along with the extracted modal peaks and theoretical predictions.

Phase velocities are numerically calculated using equation (3) and then smoothed using a moving average filter to remove high frequency fluctuation. Figure 7 shows the resulting estimates for both extracted modes.
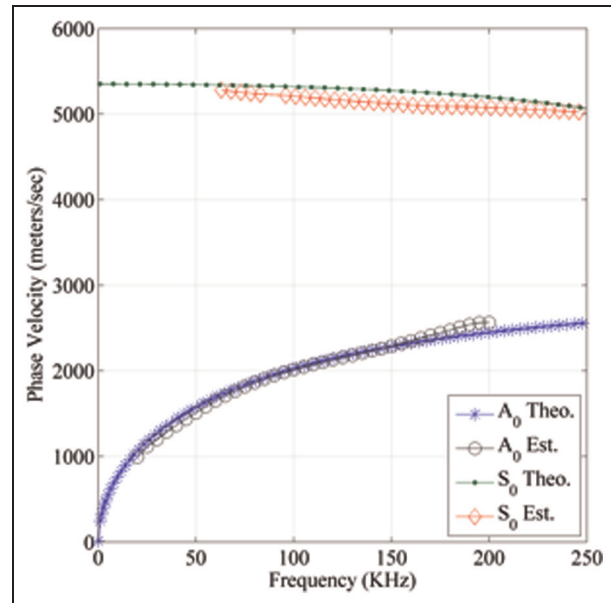
The A_0 mode, which is extremely dispersive (phase velocity increases by over 1000 m/s from 20 to 100 kHz), is in good agreement with theoretical predictions. The S_0 mode is less dispersive, but the estimated curve is offset from the theoretical prediction. The offset is attributed to error in estimation of the wavenumber peaks caused by the presence of the two modes. This is similar to spectral leakage in Fourier analysis (Harris, 1978), whereby power from the two modes spatially leak in wavenumber biasing the location of peaks. Note that at approximately 150 kHz, the S_0 mode phase velocity estimate begins to slope back toward the theoretical curve and A_0 estimate to slope away and that this transition coincides with the transition between the S_0 mode becoming dominant in power over the A_0 mode.

Several important features concerning the implementation of an active inspection method using a phased array can be drawn from Figure 6. The first is that the A_0 mode is the first to alias spatially at 200 kHz. This immediately bounds the excitation frequency range for interrogating unknown scattering sources. Even if it is possible only to excite the S_0 mode from an actuation source, the potential for aliasing mode-converted signals still exists. Here, the frequency range is extended past 200 kHz to show the S_0 mode without any affect from A_0 aliasing since the direction of arrival is known, which allows for prediction of where the aliased A_0 mode appears in the wavenumber domain. A second feature to note is the respective power of the modes and how it varies as a function of frequency contributed to the interaction of the actuator/transducer and the plate (Giurgiutiu, 2005). This is clearly seen in Figure 8, where the normalized power (peaks extracted from
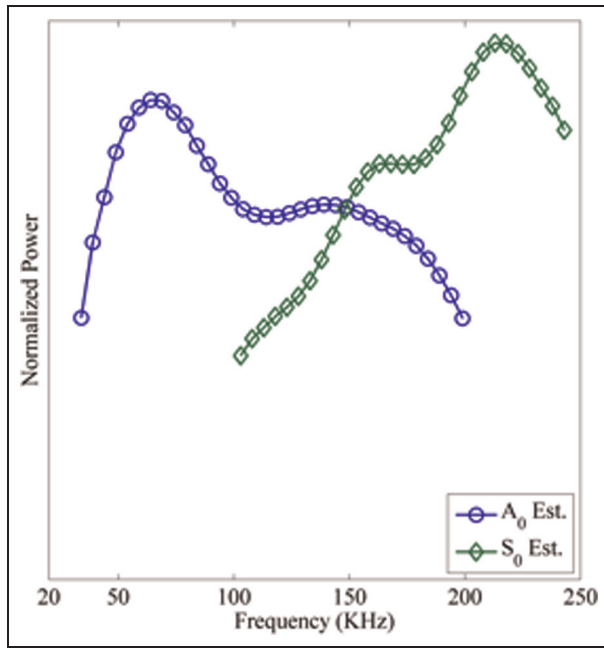
Figure 8. Extracted normalized power of antisymmetric and symmetric modes for aluminum plate.
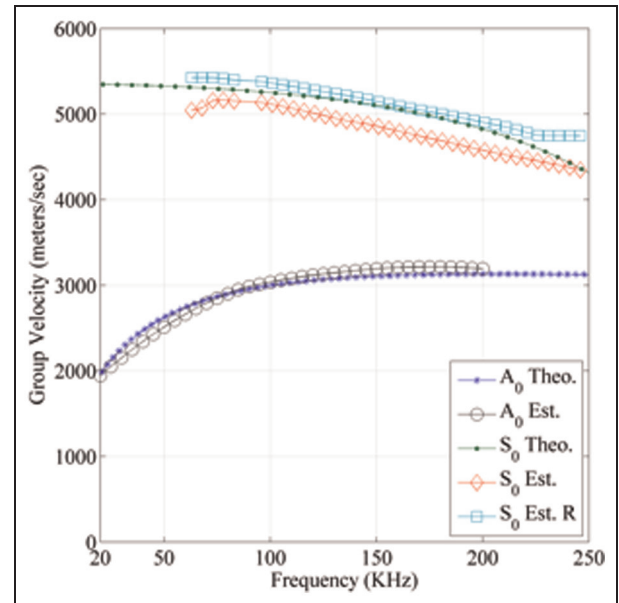

Figure 10. Theoretical (Theo.) and estimated (Est.) group velocity curves for aluminum plate. S_0 Est. is estimated from transducer waveform arrival while S_0 Est. R is estimated from wall reflection.
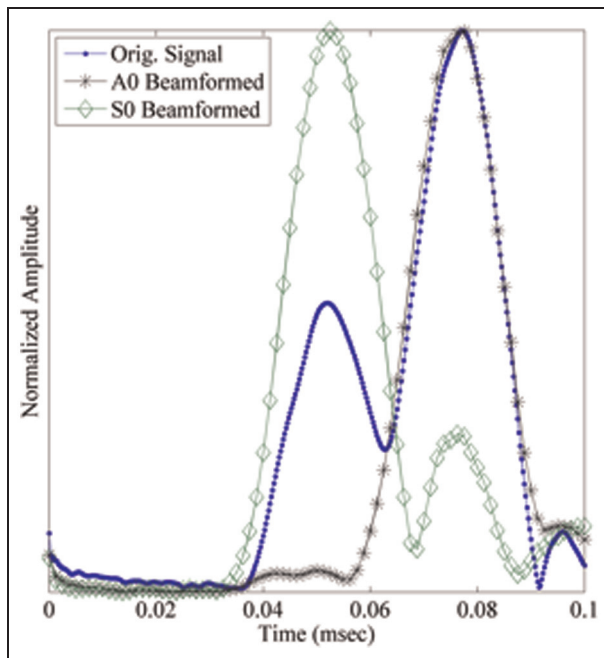

Figure 9. Separation of antisymmetric and symmetric modes in time via mode beamforming, 100 kHz excitation frequency.

Group velocity estimation. The time of flights for the A_0 and S_0 modes are estimated by beamforming for each mode using the estimated phase velocities in the direction of the actuation transducer, and then picking the peak of the resulting time series envelope. Figure 9 illustrates this for an actuation frequency of 100 kHz. Beamforming for one mode (A_0/S_0) suppresses the other (S_0/A_0), allowing for estimation of time of flight based upon peak picking. Knowing the distance traveled, group velocities curves are calculated and smoothed using a moving average filter (Figure 10). As with the phase velocity estimate, the estimated A_0 mode coincides with the theoretical prediction while the estimated S_0 mode is offset. The offset is again attributed to spectral leakage; however, this time, it is manifested as an inability to completely separate the two modes via spatial filtering (beamforming). An improved estimate is obtained using a boundary reflection instead of the direct arrival from the transducer, shown as S_0 Est. R in Figure 10. This is due to increased separation of the A_0 and S_0 modes in time. Using a known boundary reflection as the waveform source reinforces the point that to estimate phase and group velocities via the presented methods requires a source waveform from a known direction and propagation distance. This becomes particularly important when no off-array actuation transducer is used, such as the case where the phased array is used both as an excitation source and receiver. In this situation, a known reflecting source, such as a boundary reflection, can serve as the source waveform.
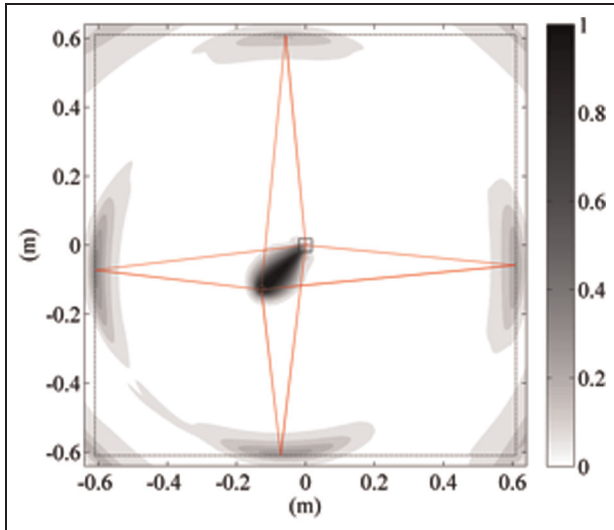
frequency–wavenumber surface of Figure 6) is plotted as a function of frequency. The A_0 mode is dominant below 150 kHz, after which the S_0 mode dominants. This provides an experimental method for the selection of narrowband excitation frequencies: excite at 60 kHz for A_0 mode and 200 kHz for the S_0 mode.

Figure 11. Antisymmetric mode average power image map for 30–150 kHz for aluminum plate.

Figure 13. Frequency–wavenumber surface for 4 × 4 array size for aluminum plate.

Figure 12. Symmetric mode average power image map for 100–240 kHz for aluminum plate.

to the imaging element and back to array center. This process is mathematically represented as

$$I\left(r, \theta, c_p, c_g\right) = \left| B(t)|_{t = t_s} \right|^2 \qquad (8)$$

Figures 11 and 12 are average image maps over the frequency ranges, where the modes are dominant in power (Figure 8). The imaging area is extended past the edge of the plate, indicated by the dotted line, to determine whether the centers of the wall reflections (shown originating from actuator and reflecting back to array) align with the plate edges. Both the A_0 and S_0 mode's reflections align at the proper locations, indicating that the phase and group velocities are close to the actual values.

Plate imaging. Using the extracted phase and group velocity curves, the A_0 and S_0 modes are beamformed and reflection/scattering sources imaged for a given narrowband actuation signal to create an image map of the plate (Ihn and Chang, 2008). This process first consists of discretizing the area of the plate into individual elements, where each element is assigned a position in range (r) and bearing (θ) relative to the array coordinate system. Scattering from each element is then imaged for each mode by (a) beamforming to the element's bearing using the mode's phase velocity and (b) assigning the element a value from the beamformed time series based upon the time of flight, t_s, for the mode with group velocity c_g to travel from the actuator
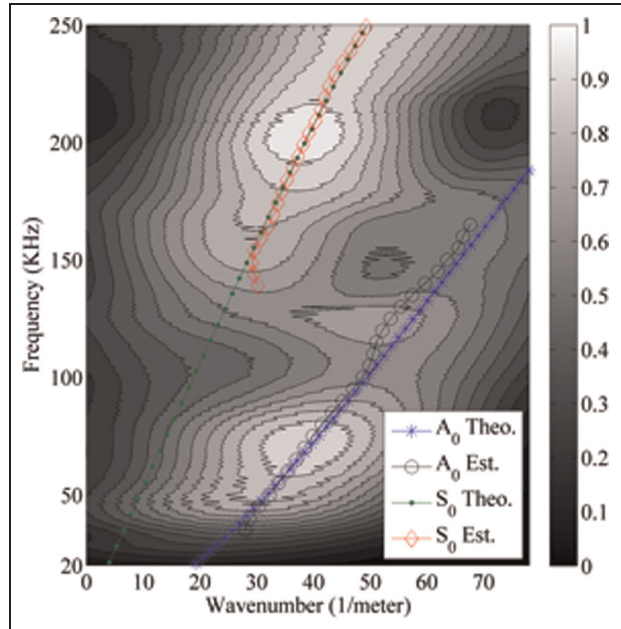
Reduction of array size. To investigate the effect of array size on estimating phase and group velocity, the 7 × 7 array is incrementally reduced in size, and the phase and group velocities are again estimated. Frequency–wavenumber surfaces for array sizes of 4 × 4, 3 × 3, and 2 × 2 are shown in Figures 13 to 15. As the array size decreases, the ability to separate the modes decreases until eventually the two modes appear as a single mode. This is particularly evident between 100 and 150 kHz for the 3 × 3 array, where the peaks from the individual modes begin to migrate toward one another. Additionally, the frequency ranges over which modes are found also decreases.

The root mean square deviation between estimated and theoretical velocity values as a function of array
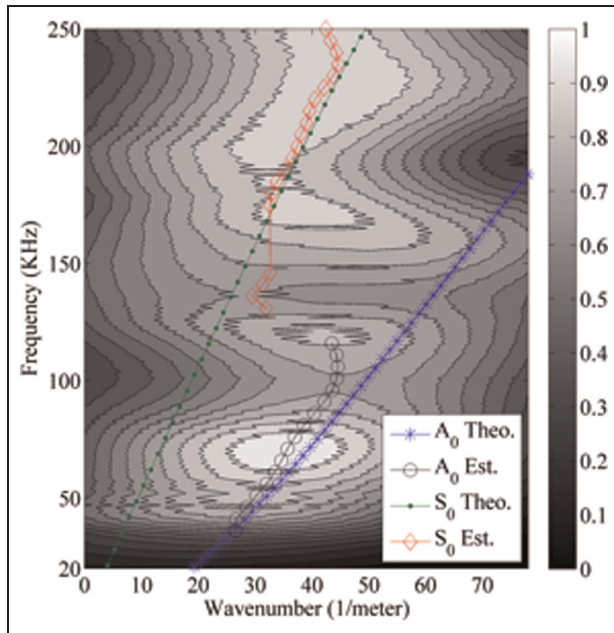
Figure 14. Frequency–wavenumber surface for 3 × 3 array size for aluminum plate.

Figure 16. RMSD between theoretical and estimated group and phase velocities for aluminum plate.
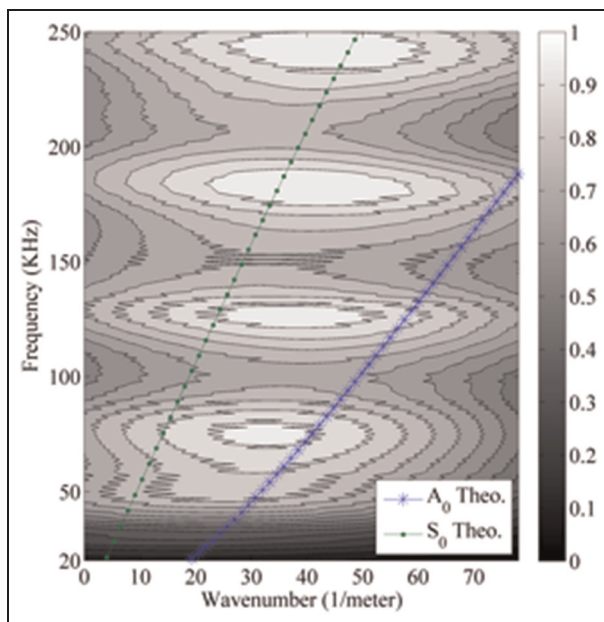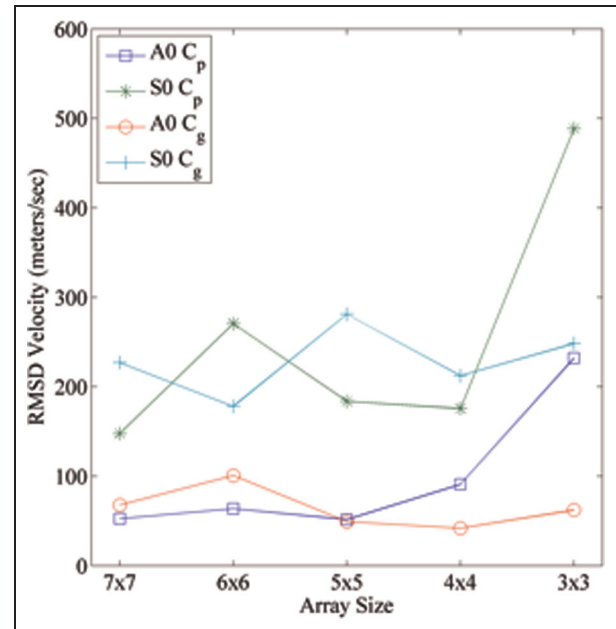RMSD: root mean square deviation.

Figure 15. Frequency–wavenumber surface for 2 × 2 array size for aluminum plate.

size is shown in Figure 16. Error in the estimated phase velocities is relatively constant until the 3 × 3 array size, when, as previously mentioned, the extracted modal peaks are pulled toward each other. Error in group velocity estimates is also relatively constant since the frequency ranges over which the modes are estimated are dominated by a single mode, allowing for the proper peak to be selected even though the modes overlap in time.

For this analysis, a 4 × 4 array is the smallest array size that could separate the A_0 and S_0 modes using an automated function that identifies the ridges of energy in the frequency–wavenumber domain and then extracts the modes. In general, the ability of an array to separate modes is a function of many variables, including the number of propagating modes, their relative difference in wavenumber and power, array weighting function, and the spatial resolution of the array. For a thorough discussion, see Johnson and Dudgeon (1993: 77–105).

Carbon fiber laminate plate

The experimental setup and plate geometry are illustrated in Figure 5. The exact material properties of the carbon fiber laminate plate in this experiment are unknown. This situation mimics many real-world applications where there is often uncertainty in material properties, layout orientation, and fabrication, particularly when monitoring an existing structure in a retrofit mode. Nine actuators are placed at a constant radial distance with 22.5° spacing to test for anisotropy with the assumption that the direction of propagation for the phase velocity coincides with the direction of propagation for the group velocity (Wang and Yuan, 2007). An example frequency–wavenumber surface is shown in Figure 17 with two modes identified as Mode 1 (20–100 kHz) and Mode 2 (60–100 kHz).

Phase velocity is iteratively estimated for each actuator as previously described in the dispersion curve
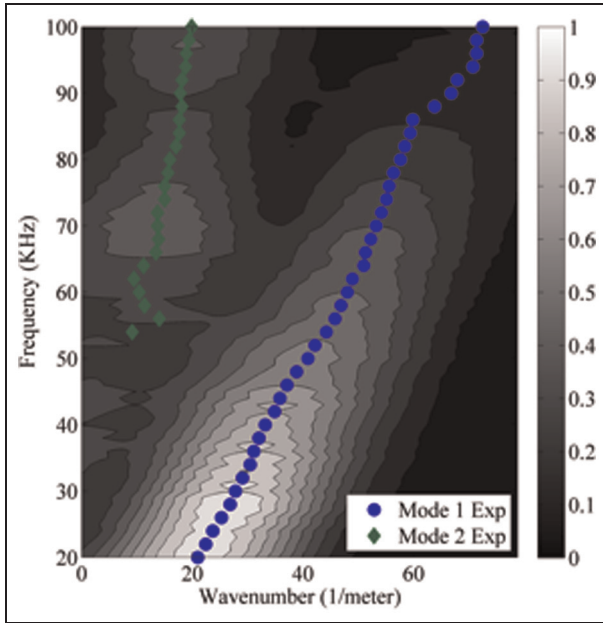
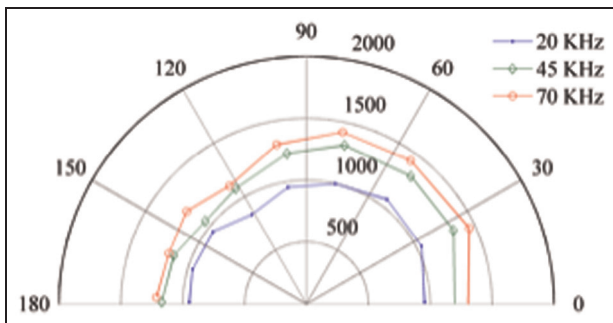**Figure 17.** Frequency–wavenumber surface for actuator at 0° for carbon fiber laminate plate.

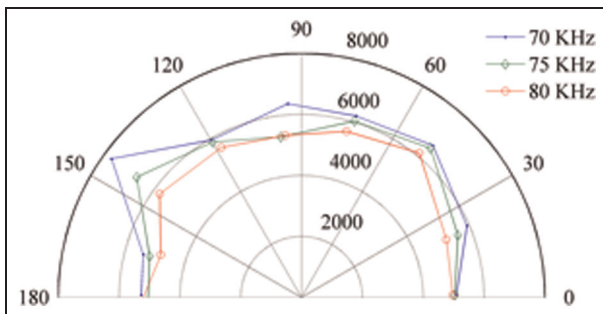**Figure 18.** Mode1 phase velocity (m/s) for carbon fiber laminate plate.

Figure 19. Mode 2 phase velocity (m/s) for carbon fiber laminate plate.

Figure 20. Mode 1 group velocity (m/s) for carbon fiber laminate plate.
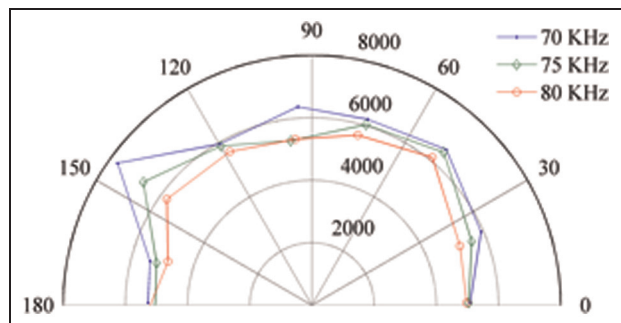
Figure 21. Mode 2 group velocity (m/s) for carbon fiber laminate plate.

a slight dependence on angle with maximum values occurring over the angles from 30° to 90°. Phase velocity for Mode 2 is fairly constant except for 135° where the estimated velocity is faster. Figures 20 and 21 are group velocity estimates where Mode 1 is again constant over all angles and Mode 2 is fastest at 135°.

The plate is imaged using the estimated phase and group velocities over the extracted frequency ranges with the image maps for actuators at 120° and 0° shown in Figures 22 and 23. The plate is imaged again with equation (8), with the exception that the directional dependence of phase and group velocity for a given reflection/propagation path, that is, the angles formed between actuator and image element and image element and array center, is taken into account through linear interpolation using the estimated velocities.

The four main boundary reflections are traced (assuming angle of incidence is equal to angle of reflection) to show alignment. The direct arrivals from the actuator, as well as boundary reflections, align well for Modes 1 and 2, indicating that the estimated phase and group velocity values are reasonably accurate.

Conclusion

Methods for estimating phase velocity (wavenumber beamforming) and group velocity (mode beamforming)

estimation section. Figures 18 and 19 show the resulting phase velocity estimates in polar form for the dominant frequencies. The phase velocity for Mode 1 shows
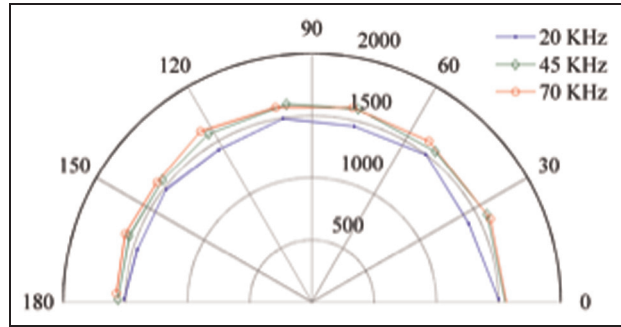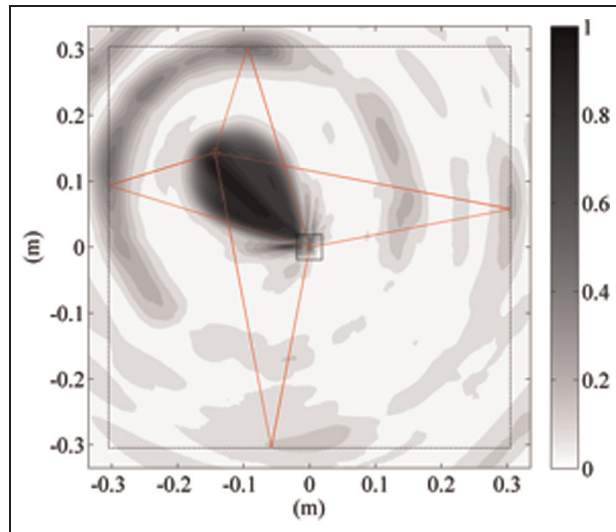
Figure 22. Mode 1 average power image map for 20–70 kHz for carbon fiber laminate plate.

Figure 23. Mode 2 average power image map for 70–80 kHz for carbon fiber laminate plate.

An additional limitation is the ability to identify and separate modes from the frequency–wavenumber surface, which is dependent upon array geometry, number of sensors, sensor spacing, and processing techniques. This was investigated experimentally for the aluminum plate with the result that a 4×4 array was the smallest array size that could accurately separate and estimate velocities. Thus, the number of sensors required to separate modes for a given array will be a limiting factor, in particular for deployed systems.

References

Alleyne D and Cawley P (1991) A two-dimensional Fourier transform method for the measurement of propagating multimode signals. *Journal of the Acoustical Society of America* 89(3): 1159–1168.

Alleyne DN and Cawley P (1992) The interaction of lamb waves with defects. *IEEE Transactions on Ultrasonics, Ferroelectrics and Frequency Control* 39(3): 381–397.

Clarke T, Cawley P, Wilcox PD, et al. (2009) Evaluation of the damage detection capability of a sparse-array guided-wave SHM system applied to a complex structure under varying thermal conditions. *IEEE Transactions on Ultrasonics, Ferroelectrics and Frequency Control* 56(12): 2666–2678.

Giurgiutiu V (2005) Tuned lamb wave excitation and detection with piezoelectric wafer active sensors for structural health monitoring. *Journal of Intelligent Material Systems and Structures* 16(4): 291–305.

Giurgiutiu V and Bao J (2004) Embedded-ultrasonics structural radar for in situ structural health monitoring of thin-wall structures. *Structural Health Monitoring* 3(2): 121–140.

Hall JS and Michaels JE (2010) A model-based approach to dispersion and parameter estimation for ultrasonic guided waves. *Journal of the Acoustical Society of America* 127(2): 920–930.

Harris FJ (1978) On the use of windows for harmonic analysis with the discrete Fourier transform. *Proceedings of the IEEE* 66(1): 51–83.

Hutchins DA, Lundgren K and Palmer SB (1989) A laser study of transient lamb waves in thin materials. *Journal of the Acoustical Society of America* 85(4): 1441–1448.

Ihn J-B and Chang F-K (2008) Pitch-catch active sensing methods in structural health monitoring for aircraft structures. *Structural Health Monitoring* 7(1): 5–19.

Johnson DH and Dudgeon DE (1993) *Array Signal Processing (Prentice Hall Signal Processing Series)*. 1st ed. Upper Saddle River, NJ: Prentice Hall Publishers.

in situ via a phased array were introduced and related to spectral decomposition of a multimodal wave field. Experiments were performed on an aluminum and carbon fiber plate. Plate wave modes were identified, associated phase and group velocities estimated, and then used to image back-scattering over broad frequency ranges.

A limitation of both wavenumber beamforming and mode beamforming is the requirement of a source waveform from a known direction. Experimentally, this was fulfilled by having an off-array actuator. A known reflection source, such as an edge reflection, can instead be used as a source but may not be possible for all applications.

Kley M, Valle C, Jacobs LJ, et al. (1999) Development of dispersion curves for two-layered cylinders using laser ultrasonics. *Journal of the Acoustical Society of America* 106(2): 582–588.

Lowe MJS (1995) Matrix techniques for modeling ultrasonic waves in multilayered media. *IEEE Transactions on Ultrasonics, Ferroelectrics and Frequency Control* 42(4): 525–542.

Michaels JE and Michaels TE (2007) Guided wave signal processing and image fusion for in situ damage localization in plates. *Wave Motion* 44(6): 482–492.

Niethammer M, Jacobs LJ, Qu J, et al. (2001) Time-frequency representations of lamb waves. *Journal of the Acoustical Society of America* 109: 1841–1847.

Prosser WH, Seale MD and Smith BT (1999) Time-frequency analysis of the dispersion of lamb modes. *Journal of the Acoustical Society of America* 105(5): 2669–2676.

Rose JL (2002) A baseline and vision of ultrasonic guided wave inspection potential. *Journal of Pressure Vessel Technology* 124(3): 273–282.

Sachse W and Pao Y-H (1978) On the determination of phase and group velocities of dispersive waves in solids. *Journal of Applied Physics* 49(8): 4320–4327.

Schumacher NA, Burger CP and Gien PH (1993) A laser-based investigation of higher-order modes in transient lamb waves. *Journal of the Acoustical Society of America* 93(5): 2981–2984.

Wang L and Yuan FG (2007) Group velocity and characteristic wave curves of lamb waves in composites: modeling and experiments. *Composites Science and Technology* 67(7–8): 1370–1384.